Analysis of high-quality modes in open chaotic microcavities

W. Fang, A. Yamilov, and H. Cao
Department of Physics and Astronomy, Northwestern University, Evanston, Illinois 60208-3112, USA
(Received 2 April 2005; published 15 August 2005)

We present a numerical study of the high-quality modes in two-dimensional dielectric stadium microcavities. Although the classical ray mechanics is fully chaotic in a stadium billiard, all of the high-quality modes show a ''strong scar'' around unstable periodic orbits. When the deformation (ratio of the length of the straight segments over the diameter of the half circles) is small, the high-quality modes correspond to whispering-gallery-type trajectories and their quality factors decrease monotonically with increasing deformation. At large deformation, each high-quality mode is associated with multiple unstable periodic orbits. Its quality factor changes nonmonotonically with the deformation, and there exists an optimal deformation for each mode at which its quality factor reaches a local maximum. This unusual behavior is attributed to the interference of waves propagating along different constituent orbits that could minimize light leakage out of the cavity.

DOI: 10.1103/PhysRevA.72.023815 PACS number(s): 42.55.Sa, 05.45.Pq, 05.45.Mt

I. INTRODUCTION

Microlasers are essential components of integrated photonic circuits. To reduce power consumption, a low lasing threshold is desired, which can be realized with microcavities of high-quality factor Q. Among the various types of semiconductor microlasers that have been developed over the past two decades, microdisk lasers have the highest-quality factors. This is because light is confined in circular dielectric disks by total internal reflection, and the only escape channel for light is evanescent tunneling whose rate is extremely small. The major drawback of microdisk lasers is undirectional (isotropic) output. To overcome this problem, deformation of the disk shape from circle was proposed [1]. Directional laser output was observed in asymmetric resonant cavities of quadrupolar deformation [2,3]. Another type of deformed cavity is Bunimovich's stadium which consists of two half circles connected by two straight segments. Different from a quadrupolar billiard, ray mechanics in a stadium billiard exhibits "full chaos"; i.e., there exist no stable periodic orbits. However, a dense set of unstable periodic orbits (UPO's) is still embedded in the chaotic orbits. Although the UPO's are found with zero probability in classical dynamics, in wave mechanics they manifest themselves in the eigenstates of the system. There exist extra and unexpected concentrations, so-called scars, of eigenstate density near UPO's [4]. Lasing has been realized in both scar modes and chaotic modes of dielectric stadium with a certain aspect ratio [5,6]. However, it is not known how the lasing modes would change when the aspect ratio of the stadium is varied gradually. When optical gain is uniformly distributed across the cavity, the lasing modes are typically the cavity modes of high-quality factor Q. Thus it is important to find out what the high-quality modes are in the stadium cavities and how their Q values depend on the cavity shape. In this paper, we present a numerical study of the high-quality modes in dielectric stadium cavities of various aspect ratios. Our results will help to predict which cavity modes would be the lasing modes under uniform pumping.

From the fundamental physics point of view, a two-dimensional (2D) stadium billiard is a well-known model for classical and quantum chaos. There have been detailed studies of the eigenmodes in closed stadium billiards—e.g., a microwave cavity where rays cannot escape [4,7–12]. Even in studies of conductance (transmission) through an open stadium billiard, only a few leads are attached to the stadium boundary through which rays can escape [13]. A dielectric stadium is very different in the sense that its entire boundary is open so that refractive escape and tunneling escape of light could happen at any point on the boundary. In terms of wave mechanics, the eigenenergies of a dielectric stadium cavity are complex numbers whose imaginary parts reflect the lifetimes of the eigenmodes. It is not clear whether the eigenmodes of a dielectric stadium can have a long lifetime and, if so, what the physical mechanism for the formation of long-lived modes is. These are the issues we intend to address in this paper.

The paper is organized as follows. Section II contains a brief description of the numerical methods used to obtain the cavity resonances and identify their corresponding classical ray trajectories. In Sec. III, two regimes of deformation for a dielectric stadium are introduced based on the characteristic of the high-Q modes. The simulation results of high-Q modes in the regime of small deformation are presented in Sec. IV, followed by the analysis of high-Q modes in the large deformation regime in Sec. V. Finally the conclusion and implication of our results are given in Sec. VI.

II. NUMERICAL METHODS

We calculated numerically the high-quality modes in 2D dielectric stadium cavities. The radius of the half circles is r, and the length of the straight segments is $2a$ (see the inset of Fig. 1). The area of the stadium is fixed while its shape is varied. We define the deformation $\epsilon \equiv a/r$. In our simulation, ϵ ranges from 0.1 to 1.6. The nonintegrable nature of the problem precludes analytical results; thus, we resorted to numerical computation in the analysis of eigenmodes in a di-

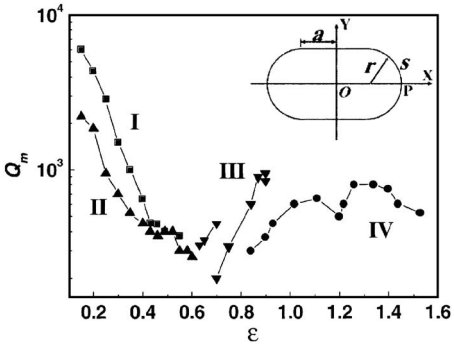

FIG. 1. Maximum quality factor Q_m of class-I, -II, -III, and -IV modes, represented by squares, up-triangles, down-triangles, and circles, as a function of deformation ϵ. The inset is a schematic of the dielectric stadium cavity.

electric stadium surrounded by vacuum. The refractive index of the dielectric $n=3$. Using the finite-difference time-domain (FDTD) method, we solved Maxwell's equations for the electromagnetic field both inside and outside the cavity. The vacuum outside the cavity is terminated by a uniaxial perfectly matched layer (UPML) that absorbs light escaping from the dielectric stadium into the vacuum. We identify and characterize all high-Q modes in the spectral range of 600–1200 nm in two-step calculations. First, a short optical pulse of broad bandwidth is launched across the cavity to excite all resonant modes in the (vacuum) wavelength range of 600–1200 nm. Photons in the low-Q modes quickly leak out of the cavity. Long after the excitation pulse is gone, photons that still stay inside the cavity must be in one of the high-Q modes. The Fourier transform of the intracavity electromagnetic field exhibits narrow spectral peaks that correspond to these long-lived modes. The linewidth of each mode reflects its Q value. Next, we repeated the FDTD calculation with quasicontinuous wave excitation at the frequency of a high-Q mode. Since only one high-Q mode is excited, the steady-state distribution of the electromagnetic field exhibits the spatial profile of this mode.

To find out the classical ray trajectories that the high-Q modes correspond to, we obtained the quantum Poincaré sections of their wave functions. We calculated the Husimi phase-space projection of a mode from its electric field at the stadium boundary. The coordinates of the Husimi map are s and $\sin\chi$. s is the length along the boundary of the stadium from point P (see the inset of Fig. 1), normalized to the perimeter of the stadium. $\sin\chi \equiv k_{\|}/k$, where $k_{\|}$ is the k vector in the direction tangent to the stadium boundary, $k=2\pi n/\lambda$, and λ is the wavelength in vacuum.

III. TWO REGIMES OF DEFORMATION

We have considered both transverse electric (TE) and transverse magnetic (TM) polarization and obtained similar results in our calculation. The data presented in the following are for the TM polarizations. Starting with a perfect circle, we gradually increased the deformation ϵ while keeping the area of the stadium at 3.3 μm^2. In the range of ϵ from 0.1 to 1.6, we identified four classes of high-Q modes in the (vacuum) wavelength range of 600–1200 nm. Figure 1 shows their maximum quality factor Q_m as a function of ϵ. Within each class, the highest-Q modes at different ϵ may not be the same mode. As ϵ increases, Q_m first decreases quickly, reaches a minimum at $\epsilon \sim 0.6$, and then starts increasing before reaching a plateau at large ϵ. Hence, $\epsilon \sim 0.6$ seems to be a turning point, across which the spatial profiles of the high-Q modes also change significantly. Based on these phenomena, we divided the deformation into two regimes. In the regime of small deformation ($\epsilon \lesssim 0.6$), Q_m decreases monotonically as ϵ increases. As will be shown in the next section, the high-Q modes in this regime, labeled as class I and class II, have field maxima only near the stadium boundary. In the regime of large deformation ($\epsilon \gtrsim 0.6$), Q_m first increases with ϵ and then remains nearly constant with small oscillations after ϵ exceeds 0.9. The high-Q modes in this regime, labeled as class III and class IV, exhibit very different spatial profiles from those at small deformation. As will be shown in Sec. V, they have field maxima not only close to the boundary, but also near the center of the stadium. Therefore, across the boundary ($\epsilon \sim 0.6$) of the above two regimes, the characteristic of the high-Q modes changes dramatically; in other words, different types of eigenmodes take over as the high-Q modes. In the following a systematic study of the high-Q modes in the two regimes of deformation is presented.

IV. HIGH-Q MODES IN THE REGIME OF SMALL DEFORMATION

We used short-pulse excitation to find all the high-Q modes in the (vacuum) wavelength range of 600–1200 nm for $\epsilon \lesssim 0.6$. Figure 2(a) is the spectrum of electromagnetic field inside the stadium of $\epsilon=0.15$ long after the short-pulse excitation is gone. There are two groups of high-Q modes. Within each group, the modes have similar spatial profiles. The group of class-I modes is at shorter wavelength, while the group of class-II modes at longer wavelength. Using the quasicontinuous wave excitation, we studied individual high-Q modes. Figure 3(a) shows the spatial intensity distribution of a class-I mode at $\epsilon=0.15$. It is clear that the class-I mode is not a chaotic mode, but a scar mode. To identify the classical ray trajectories that the class-I modes correspond to, we calculated the quantum Poincaré sections of their wave functions. Figure 3(b) is the Husimi phase-space projection of the class-I mode shown in Fig. 3(a). The main features are four "pads," which correspond to the rectangle orbit as illustrated in the inset of Fig. 3(b). Above the four pads, there is a "belt" which may represent long orbits that slide along the stadium boundary. Moreover, the Husimi function has zero points near the diamond orbit [marked by crosses in Fig. 3(b)].

Similarly, the class-II modes are also scar modes [Fig. 4(a)]. As shown in Fig. 4(b), the Husimi map of a class-II mode consists of four "pads" that correspond to the diamond orbit and a "belt" on top of it. It also reveals four zero points of the Husimi function near the rectangle orbit [marked by dots in Fig. 4(b)]. It is not clear why class-I modes form a group of high-Q modes in the wavelength region around 700 nm, while the class-II modes form a group of high-Q

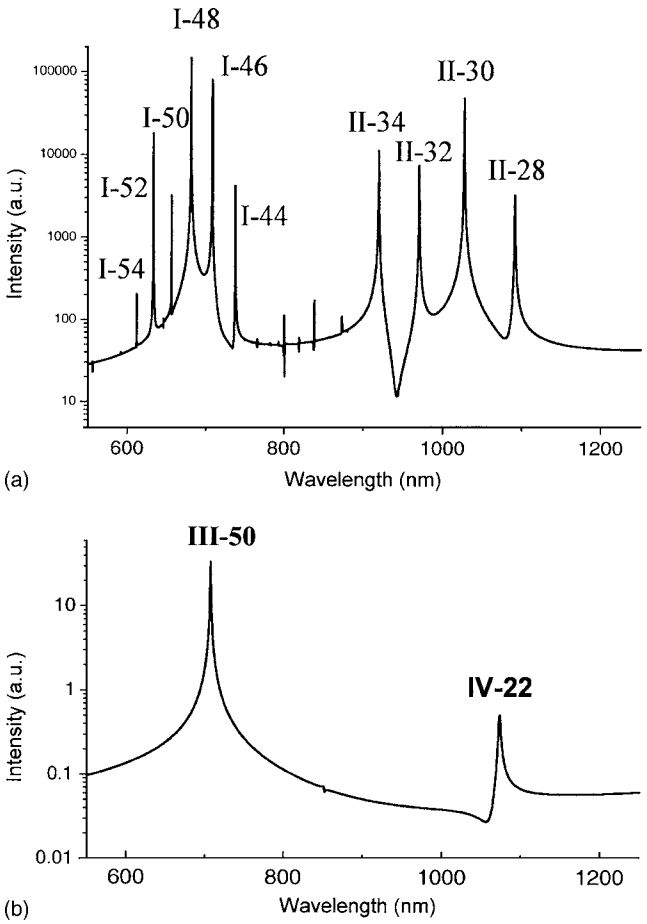

FIG. 2. Spectra of electromagnetic field inside the dielectric stadium long after the short-pulse excitation is gone. (a) $\epsilon=0.15$. (b) $\epsilon=0.84$.

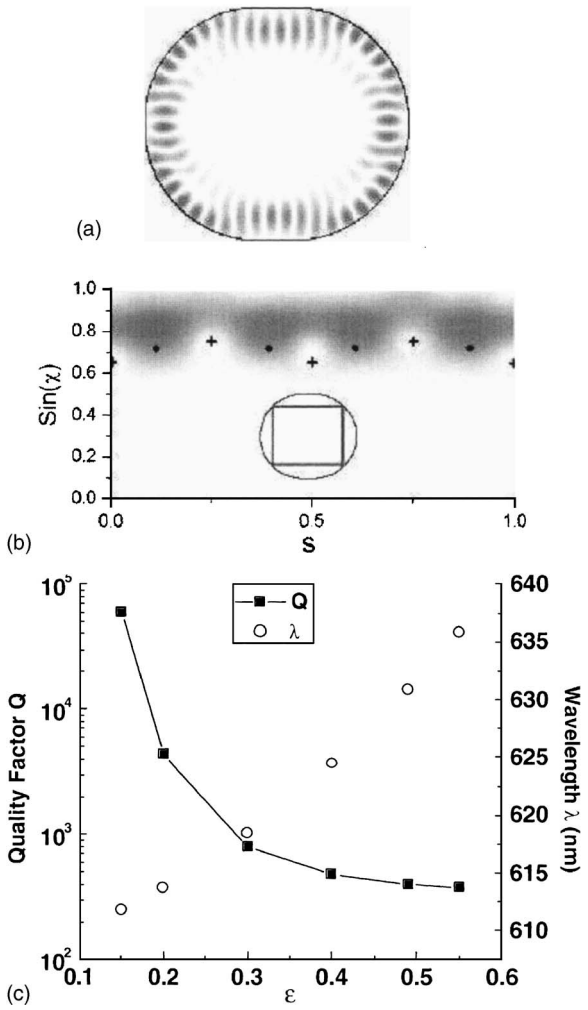

FIG. 3. (a) Spatial intensity distribution of a class-I mode in the dielectric stadium of $\epsilon=0.15$. (b) Husimi phase-space projection of the mode in (a). The black dots represent the rectangle orbit, which is shown schematically in the inset. The crosses correspond to the diamond orbit. (c) Quality factor Q (solid squares) and wavelength (open circles) of the mode in (a) as a function of the deformation ϵ.

modes around $\lambda \sim 1000$ nm. We notice that within each group of high-Q modes, the frequency spacing between adjacent modes is constant. Individual modes can be labeled by the number of field maxima N along the stadium boundary, as shown in Fig. 2(a). N is an even number due to the symmetry of the wave function with respective to the horizontal x axis and the vertical y axis. We compared the quality factor of individual modes within a group of high-Q modes. The modes located spectrally near the group center always have higher Q values than those away from the center. The small peaks around $\lambda=800$ nm in Fig. 2(a) are class-I or -II modes with lower Q factor. Hence, the Q factor reaches the maximum at the group center.

To find out how the class-I (-II) modes change with the deformation, we traced individual modes as we gradually varied ϵ. Figure 3(c) [4(c)] shows the calculation result for the class-I (-II) mode in Fig. 3(a) [4(a)]. When ϵ increases, the mode shifts to longer wavelength, and its Q value decreases. The wavelength shift is caused by an increase in the stadium perimeter with ϵ as the area of the stadium remains constant. We repeated the calculation with different class-I (-II) modes and observed similar behaviors.

V. HIGH-Q MODES IN THE REGIME OF LARGE DEFORMATION

In the regime of large deformation $\epsilon \gtrsim 0.6$, we again found all the high-Q modes in the (vacuum) wavelength range of 600–1200 nm with the short-pulse excitation. Figure 2(b) shows the spectrum in the stadium of $\epsilon=0.84$ long after the short-pulse excitation is gone. The high-Q modes are sparse compared to the case of small deformation. Based on their intensity distributions in real space and phase space, we classified the high-Q modes into two categories, class III and class IV. Figures 5 (6) exhibits the spatial intensity distributions of two class-III (-IV) modes. These modes have field maxima not only close to the boundary, but also in the center of the stadium. The class-III mode has a structure of a "double pentagon" and class-IV mode a "double circle." The double-circle modes have been observed previously in the stadium-shaped microwave billiard and dielectric cavity

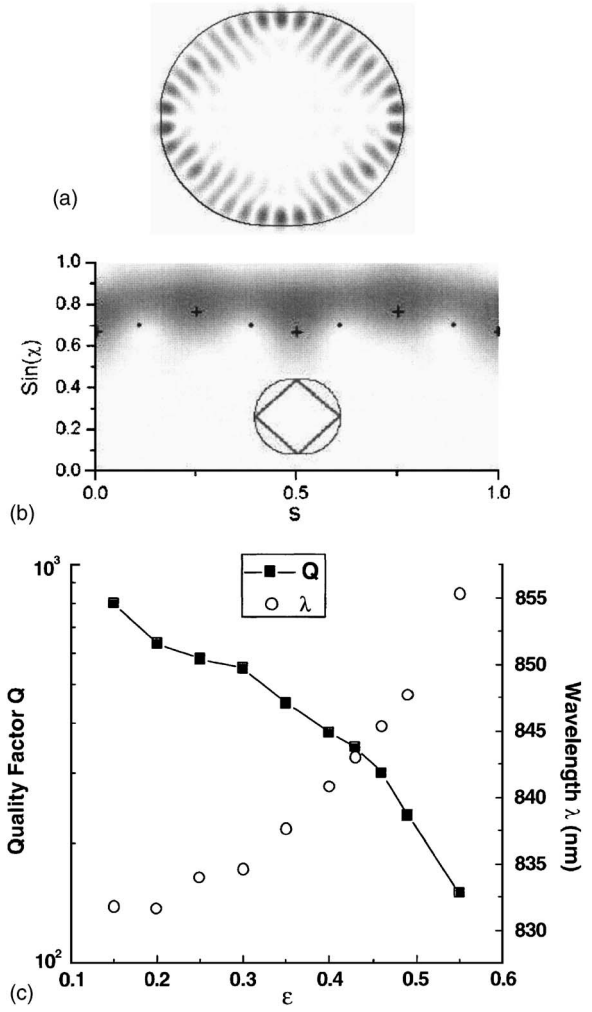

FIG. 4. (a) Spatial intensity distribution of a class-II mode in the dielectric stadium of ϵ=0.15. (b) Husimi phase-space projection of the mode in (a). The crosses represent the diamond orbit, which is shown schematically in the inset. The black dots correspond to the rectangle orbit. (c) Quality factor Q (solid squares) and wavelength (open circles) of the mode in (a) as a function of the deformation ϵ.

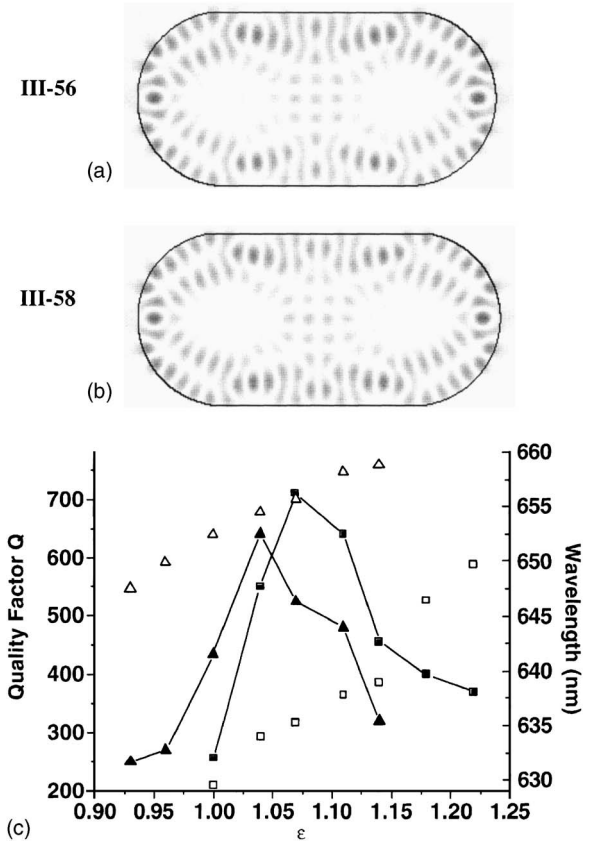

FIG. 5. (a) and (b) are spatial intensity distributions of two adjacent class-III modes of order N=56 and 58 at their optimal deformations. (c) Solid squares (triangles) and open squares (triangles) represent the quality factor and wavelength of mode III-56 (III-58).

[10,14]. What is not known before is the change of their quality factor with deformation ϵ. Figure 5(c) [6(c)] shows how the Q values of individual class-III (-IV) modes vary with ϵ near ϵ=1.0. For each mode, its Q value first increases with ϵ and then decreases. There exists an optimal deformation ϵ_m for each mode at which its quality factor reaches the maximum. Figure 5(c) [6(c)] also shows that the wavelengths of individual class-III (-IV) modes increase with ϵ. This behavior is similar to that of class-I and class-II modes.

The two modes of class III (IV), shown in Fig. 5 (6), have the same profile except that the number of field maxima is different. We label the modes in terms of the number of field maxima, N, along the stadium boundary. The two modes in Figs. 5(a) and 5(b) are labeled as III-56 and III-58, and the two modes in Figs. 6(a) and 6(b) are IV-28 and IV-30. Because the stadium has symmetries about the x and y axes, N is always an even number. The two modes in Fig. 5 (6) are adjacent modes, as their N numbers differ by 2. The higher the N, the shorter the wavelength. After the mode of order N reaches its maximum Q at certain ϵ, a further increase of ϵ sees the mode of order $N+2$ in the same class takes over as the high-Q mode. Its Q value reaches the maximum at larger deformation. Hence, within class-III or class-IV modes, the high-Q mode hops from the mode of lower N consecutively to the one of higher N as ϵ increases. Since the higher-N modes have shorter wavelength, the high-Q mode jumps to shorter wavelength. This behavior is clearly seen in Fig. 7 for the class-IV modes when ϵ increases in small steps from 0.96 to 1.07. Individual modes shift slightly to longer wavelength as ϵ increases. Yet the high-Q mode migrates to shorter wavelength, forming a "high-Q band" with increasing ϵ. Figure 8 shows the optimal deformation ϵ_m and the corresponding wavelength for each class-IV mode in this high-Q band. The modes are antisymmetric with respective to the horizontal x axis, while their symmetry to the vertical y axis alternates between odd and even.

The nonmonotonic change in the Q value of a high-quality mode with ϵ and the existence of an optimal deformation for maximum Q have not been reported before. To explain these phenomena, we intend to understand the mode structures and their corresponding classical ray trajectories. As an example, we consider a class-IV mode, whose intensity distribution is shown in Fig. 9(a). Figure 9(c) is the Husimi phase-space projection of this class-IV mode at its

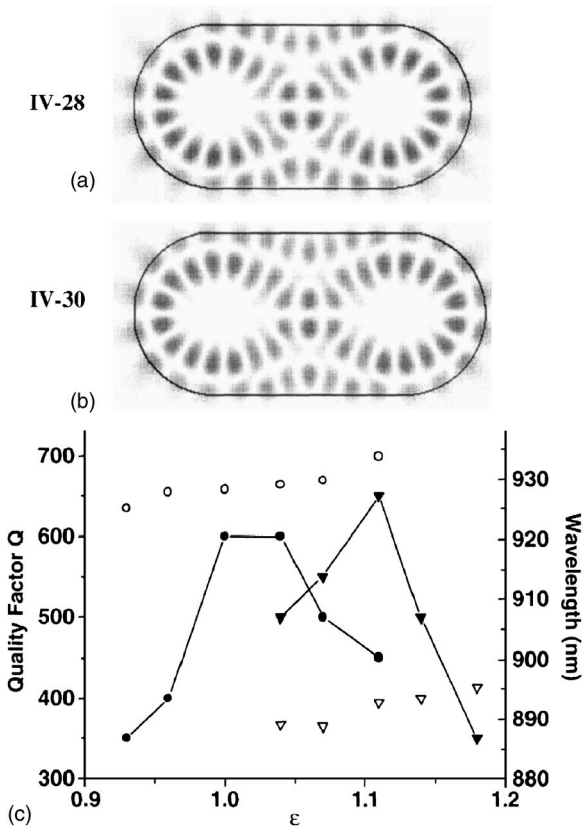

FIG. 6. (a) and (b) are spatial intensity distributions of two adjacent class-IV modes of order $N=28$ and 30 at their optimal deformations. (c) Solid circles (triangles) and open circles (triangles) represent the quality factor and wavelength of mode IV-28 (IV-30).

optical deformation $\epsilon_m=1.04$. It reveals that the class-IV mode consists mainly of two topologically distinct short periodic orbits: one is the diamond orbit [marked by black dots in Fig. 9(c)], and the other is the bow-tie orbit [marked by crosses in Fig. 9(c)]. This result illustrates that the class-IV mode is still a scar mode. Note that scarring was introduced as a term for nonuniform field patterns in systems like the stadium, because they were unexpected in the short-wavelength limit where ray physics dominated the cavity properties. In the small cavities we simulated, the wavelength was not short enough to apply the random-matrix theory and the wave solutions exhibited regular spatial patterns. Yet in the range of nkR that we studied, most low-Q modes fill more or less uniformlly the entire real space and phase space. These modes are regarded as chaotic modes. In contrast, the class-IV mode, as shown in Fig. 9, exhibits a nonuniform distribution in real space and phase space; thus, it can be considered as a scar mode. Its corresponding periodic orbits are above the critical line for refractive escape ($\sin\chi=1/3$). These orbits, which are unstable in the closed stadium, remain unstable in the open stadium owing to small light leakage and long dwell time inside the cavity. However, the measure of orbit instability—i.e., the Lypounov exponent—is changed due to the open boundary condition. Because the class-IV mode is a multiorbit scar mode, the interference of waves propagating along the constituent orbits shown in Fig. 9(b) could minimize light leakage out of the cavity [15,16]. The interference effect depends on the phases of waves traveling in different orbits. Because the phase delay varies with the orbit length which is a function of ϵ, the interference effect may be optimized at certain deformation that gives the maximum Q value.

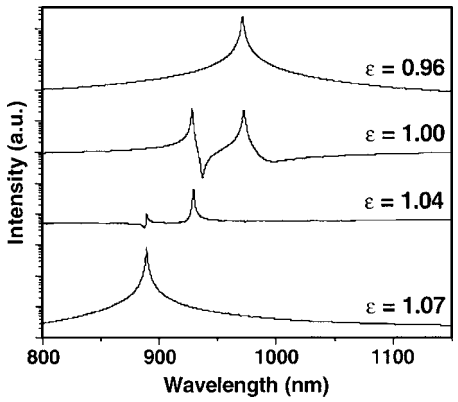

FIG. 7. Intracavity excitation spectra long after the short-pulse excitation is gone. ϵ increases in small steps from 0.96 to 1.07.

Next we present a possible explanation for the hopping of the high-Q modes to shorter wavelength with increasing ϵ. To find the wavelength of a multiorbit scar mode, we applied the quantization rule to all the constituent orbits. Taking class-IV modes as an example, we utilized the Bohr-Sommerfeld quantization rule for the constituent diamond and bow-tie orbits to determine the wave number $k=2\pi n/\lambda$. Due to the relatively small kR values of the class-IV modes in our calculation, we consider only the resonances with the lowest excitation in the transverse direction of the orbit. In other words, we only need to quantize the longitudinal motion of ray along the orbit [17]. The quantization rule for the diamond orbit is $k_dL_d+\Sigma_{i=1}^{4}\phi_i-\nu_d\pi/2=2\pi m_d$, where k_d is the wave number, L_d is the length of the diamond orbit, ϕ_i is the phase shift acquired during the ith bounce of the orbit with the stadium boundary, ν_d is the number of conjugate points along the diamond orbit, and m_d

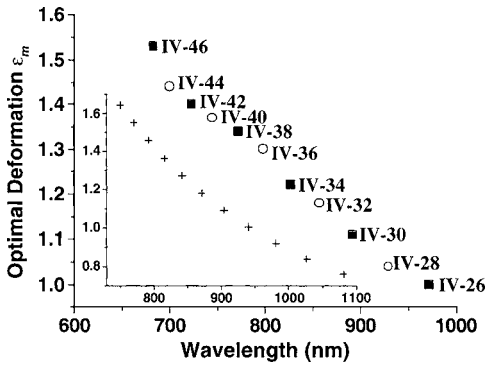

FIG. 8. Optimal deformation ϵ_m and corresponding wavelength for each class-IV mode in a high-Q band. Solid squares (open circle) represent the modes of even (odd) symmetry about the y axis. The inset shows the semiclassical prediction of wavelengths (in units of nm, horizontal axis) of class-IV modes at various deformations (vertical axis) in dielectric stadium cavities.

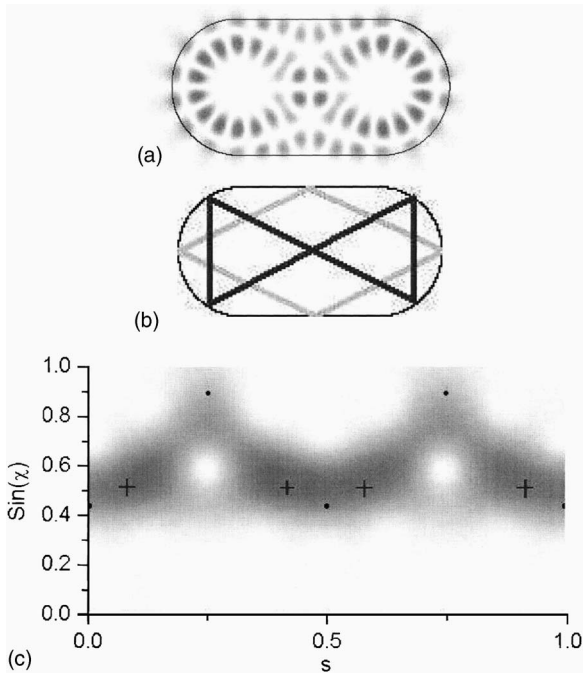

FIG. 9. Intensity distribution in real space (a) and phase space (c) of mode IV-28 at its optimal deformation $\epsilon_m=1.04$. (b) is a schematic of the constituent UPO's. The black dots (crosses) in (c) correspond to the diamond (bow-tie) orbit.

is an integer. Note that ϕ_i depends on the incident angle χ of the ray on the stadium boundary, which varies with ϵ [18]. ν_d is equal to the number of bounces with the half circles. For the diamond orbit, $\nu_d=2$. Similarly, the quantization rule for the bow-tie orbit is $k_bL_b+\Sigma_{i=1}^{4}\varphi_i-\nu_b\pi/2=2\pi m_b$, where k_b is the wave number, L_b is the length of the bow-tie orbit, φ_i is the phase shift acquired during the ith bounce of the orbit with the stadium boundary, ν_b is the number of conjugate points along the bow-tie orbit which is equal to 4, and m_b is an integer. If the coupling between the constituent orbits is neglected, the class-IV modes exist only when the quantized wave numbers of the two orbits coincide—i.e., $k_d=k_b$. We solved $k_d=k_b$ in the wavelength range of 600–1200 nm at various deformations. The inset of Fig. 8 shows the wavelength that satisfies $k_d=k_b$ as a function of ϵ. As ϵ increases, the wavelength decreases. Because the coupling between the constituent orbits is neglected, the wavelength determined by the quantization rule deviates from that obtained by the numerical simulation [19,20]. Nevertheless, the blueshift of the class-IV high-Q modes with increasing ϵ agrees qualitatively with the prediction of the semiclassical quantization rule.

The class-III modes behave very much like the class-IV modes. Similar analysis reveals that the class-III modes are also multiorbit scar modes (i.e., consisting of multiple topologically distinct short UPO's). Finally we studied the high-Q modes in the crossover regime of $\epsilon\sim0.6$. When ϵ increases and approaches the turning point of 0.6, the "belts" in Figs. 3(c) and 4(c) gradually disappear from class-I and -II modes; meanwhile, additional components corresponding to non-WG-type short UPO's start emerging in the Husimi map.

VI. CONCLUSION

We have presented a systematic study of the high-quality modes in dielectric stadium microcavities of various deformations. Despite the unstable periodic orbits having zero measure in the fully chaotic stadium billiards, all the high-Q modes are found to be scar modes. The chaotic modes have lower Q factors, because their relatively uniform distribution in the phase space facilitates the refractive escape of light from the dielectric stadium. In the regime of small deformation ($\epsilon\lesssim0.6$), we identified two classes of high-Q modes. They are scar modes that correspond to whispering-gallery-type trajectories, and their Q values decrease monotonically with increasing ϵ. The characteristic of high-Q modes changes dramatically when ϵ exceeds a critical value (~0.6). In the regime of large deformation ($\epsilon\gtrsim0.6$), the high-Q modes are still scar modes, but they are made of several topologically distinct short UPO's, some of which are not whispering-gallery type. The interference among waves propagating along different orbits can minimize light leakage out of the cavity. For each mode, there exists an optimal deformation at which its quality factor reaches a local maximum. When ϵ increases, the high-Q mode hops within the same class of modes from the lower-order one to the higher-order one. This behavior results in the formation of high-Q bands that shift to shorter wavelength with increasing ϵ.

For comparison, we also calculated the high-quality modes of an open integral system (dielectric elliptical cavity) and a partially chaotic system (dielectric quadrupolar cavity). These modes do not exhibit a nonmonotonic change of their quality factors with the deformation; neither do they have optimal deformations at which their Q values are maximized. Whether the behaviors of the high-quality modes observed in the dielectric stadium cavities are unique characteristic of fully chaotic systems requires further study.

Finally we discuss the implication of our results to the design of microlasers. For many applications of microlasers, large deformation of cavity shape from circle is desired for directional output. However, the spoiling of the Q factor in the deformed cavity results in an increase of the lasing threshold. Our calculation demonstrates that in the dielectric stadium microcavities the Q spoiling would stop after the deformation exceeds a critical value. This behavior leads to a decent lasing threshold even at large deformation. Note that our results are obtained with the calculation over a wide spectral range. The commonly used semiconductor gain media have much narrower gain spectra. Since the high-Q modes at large deformation are sparse, the chance of having a high-quality scar mode within the gain spectrum is rather low. If the high-Q scar modes do not overlap with the gain spectrum, lasing may occur in the low-Q chaotic modes located within the gain spectrum but with much higher lasing threshold. Therefore, to reach a low lasing threshold, one must carefully choose the size and deformation of the stadium so that a high-Q mode lies within the gain spectrum. Because of the low density of high-quality modes at large deformation, it is easy to realize single-mode lasing, which has potential application to single-mode lasers.

ACKNOWLEDGMENTS

We acknowledge Professor Peter Braun, Professor E. E. Narimanov, Professor F. Haake, Professor G. Casati, Professor T. Prosen, Dr. G. G. Carlo, and Dr. G. Hackenbroich for stimulating discussions. This work is supported by the MRSEC program of the National Science Foundation (Grant No. DMR-00706097) at the Materials Science Center of Northwestern University.

[1] J. U. Nockel and A. D. Stone, Nature (London) **385**, 45 (1997).
[2] S. C. Chang, J. U. Nockel, R. K. Chang, and A. D. Stone, J. Opt. Soc. Am. B **17**, 1828 (2000).
[3] C. Gmachl, F. Capasso, E. E. Narimanov, J. U. Nockel, A. D. Stone, J. Faist, D. L. Sivco, and A. Y. Cho, Science **280**, 1556 (1998).
[4] E. J. Heller, Phys. Rev. Lett. **53**, 1515 (1984).
[5] T. Harayama, T. Fukushima, P. Davis, P. O. Vaccaro, T. Miyasaka, T. Nishimura, and T. Aida, Phys. Rev. E **67**, 015207(R) (2003).
[6] T. Harayama, P. Davis, and K. S. Ikeda, Phys. Rev. Lett. **90**, 063901 (2003).
[7] M. C. Gutzwiller, *Chaos in Classical and Quantum Mechanics* (Springer, Berlin, 1990).
[8] S. W. McDonald and A. N. Kaufman, Phys. Rev. A **37**, 3067 (1988).
[9] S. Tomsovic and E. J. Heller, Phys. Rev. Lett. **67**, 664 (1991).
[10] J. Stein and H.-J. Stockmann, Phys. Rev. Lett. **68**, 2867 (1992).
[11] F. Borgonovi, G. Casati, and B. Li, Phys. Rev. Lett. **77**, 4744 (1996).
[12] G. Casati and T. Prosen, Phys. Rev. E **59**, R2516 (1999).
[13] R. G. Nazmitdinov, K. N. Pichugin, I. Rotter, and P. Seba, Phys. Rev. B **66**, 085322 (2002).
[14] S.-Y. Lee, M. S. Kurdoglyan, S. Rim, and C.-M. Kim, Phys. Rev. A **70**, 023809 (2004).
[15] T. Fukushima, J. Lightwave Technol. **18**, 2208 (2000).
[16] T. Fukushima, T. Harayama, P. Davis, P. O. Vaccaro, T. Nishimura, and T. Aida, Opt. Lett. **28**, 408 (2003).
[17] E. G. Vergini and G. G. Carlo, J. Phys. A **33**, 4717 (2000).
[18] H. E. Tureci, H. G. L. Schwefel, and A. D. Stone, Opt. Express **10**, 752 (2002).
[19] E. G. Vergini and G. G. Carlo, J. Phys. A **34**, 4525 (2001).
[20] G. G. Carlo, E. G. Vergini, and P. Lustemberg, J. Phys. A **35**, 7965 (2002).